Exp Fluids (2014) 55:1648
DOI 10.1007/s00348-013-1648-6

RESEARCH ARTICLE

The onset of cavitation during the collision of a sphere with a wetted surface

M. M. Mansoor · J. Uddin · J. O. Marston · I. U. Vakarelski · S. T. Thoroddsen

Received: 14 August 2013 / Revised: 24 October 2013 / Accepted: 10 December 2013 / Published online: 5 January 2014

Abstract We investigate the onset of cavitation during the collision of a sphere with a solid surface covered with a layer of Newtonian liquid. The conventional theory dictates cavitation to initiate during depressurization, i.e. when the sphere rebounds from the solid surface. Using synchronized dual-view high-speed imaging, we provide conclusive experimental evidence that confirms this scenario—namely—that cavitation occurs only after the sphere makes initial contact with the solid surface. Similar to previous experimental observations for spheres released above the liquid surface, bubbles are formed on the sphere surface during entry into the liquid layer. These were found to squeeze radially outwards with the liquid flow as the sphere approached the solid surface, producing an annular bubble structure unrelated to cavitation. In contrast, spheres released below the liquid surface did not exhibit these patterns.

Electronic supplementary material The online version of this article (doi:10.1007/s00348-013-1648-6) contains supplementary material, which is available to authorized users.

M. M. Mansoor · J. O. Marston (✉) · I. U. Vakarelski · S. T. Thoroddsen
Division of Physical Sciences and Engineering, King Abdullah University of Science and Technology, Thuwal 23955-6900, Saudi Arabia
e-mail: jeremy.marston@kaust.edu.sa

J. Uddin
School of Mathematics, University of Birmingham, Edgbaston B15 2TT, United Kingdom

1 Introduction

The collision of an immersed particle with a wall has been the subject of extensive research owing to its practical relevance to several industrial and natural applications such as filtration, coagulation, erosion, and sedimentation. As the immersed spherical particle slowly approaches the surface, the liquid squeezes between the narrowing gap so as to provide a lubrication force (Brenner 1961), given by $F_l = 6\pi\mu R_0^2\dot{h}/h$, where μ is the liquid viscosity, R_0 is the sphere radius, h is the separation gap, and $\dot{h}$ is the rate of approach (i.e. the sphere speed). Above a threshold impact velocity, this lubrication force becomes strong enough to deform the sphere enabling it to rebound after momentarily coming to rest (without contacting the wall for sufficiently low initial sphere inertia) as the stored elastic strain energy converts back to kinetic energy (Davis et al. 1986, 2002; Barnocky and Davis 1988; Marston et al. 2010). This is referred to as the elastohydrodynamic model which was experimentally verified by Barnocky and Davis (1988). As the sphere reverses its direction of motion upon rebound, the liquid near the sphere surface undergoes high tensile stresses when it is sucked back into the growing gap between the solid surfaces. This causes depressurization under the centre of the sphere which induces cavitation, as shown experimentally by Marston et al. (2011). Other studies (Chen and Israelachvili 1991; Kuhl et al. 1994) have provided experimental evidence that this extensional stress has to cross a certain threshold for cavitation to occur, whilst a comprehensive review of the criterion for cavitation is found in Joseph (1998) and suggested that it will occur once the tensile stress in a liquid which could not withstand tension exceeded one atmospheric pressure. The possibility of cavitation induced by shear stress was also

proposed on theoretical grounds. In this scenario, as the liquid is squeezed out of the diminishing gap during sphere approach to the wall, it could be pulled open by tension in the direction defined by the principal stresses. A recent paper claiming experimental evidence of this phenomenon is found in Seddon et al. (2012) for Newtonian fluids at low and moderate sphere impact velocities and is believed to be the first in existence. However, only one qualitative example is provided therein, which suffers from relatively low temporal and spatial resolution imaging. The previous results of Marston et al. (2011), showing cavitation only after rebound, are in accord with the previous theoretical developments in this process (Davis et al. 1986, 2002; Barnocky and Davis 1988; Marston et al. 2010) since the cavitation patterns were only observed *after* the Hertzian contact ring was observed. In addition, extensive experimental observations of a sphere approaching a wall in Marston et al. (2011), Uddin et al. (2012) never resulted in cavitation during the approach stage. In light of the apparent contradictory observations between Marston et al. (2011a, b), Uddin et al. (2012) and Seddon et al. (2012), we attempt herein to decipher the first point in time, or equivalently, sphere position relative to the solid surface, of cavitation inception as an immersed sphere approaches and rebounds from a wall. We approach the problem using synchronized dual-view (side and bottom) high-speed imaging, in contrast to single-view (bottom) imaging performed in past studies (Marston et al. 2011; Seddon et al. 2012) neither of which can claim to reveal the exact sphere position at the time of cavitation onset. We also perform numerical simulations based on a published model of this process to assess the shear stress as a function of gap height.

2 Experimental setup

A schematic of the experimental setup used is shown in Fig. 1. The sphere made from tungsten carbide (Fritsch GmbH, Germany, $\rho_s = 14,890$ kg/m^3, $E = 550$ GPa) is released using an electromagnet positioned directly above the centre of a thick glass container having a base measuring 100 × 100 × 20 mm. The choice of tungsten carbide ensured a matt surface, thus eliminating reflections from the sphere surface throughout the experiments. In order to ensure that the glass container does not oscillate when subjected to impacts, it is fixed firmly to a solid stainless steel frame weighing approximately 10 kg, which in turn was bolted directly to a 1,000-kg optical table. The U-shaped frame had space to accommodate a mirror angled at 45° to allow observations from underneath the sphere. The events were recorded from the side and bottom at 33,000 fps using two synchronized high-speed cameras

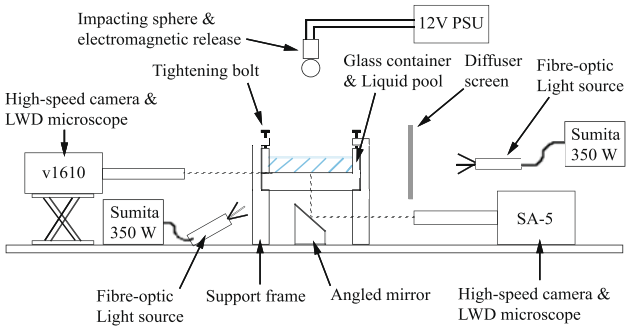

Fig. 1 Schematic of the experimental setup

each equipped with a long-working distance microscope. These included a Photron SA-5 and a Phantom v1610 with effective pixel resolutions of 448 × 448 and 1,275 × 400 pixels, respectively. The Phantom camera auto-triggered the recordings (using the IBAT function) upon sensing motion at the top of the side field of view. Each set of video clips was saved to a PC for subsequent analysis. Two 350 W Sumita metal halide light sources each equipped with fibre-optic guides were used to provide lighting. These induced minimal heating to the liquid, as checked by temperature measurements. The experiments were conducted in a controlled environment with a relative humidity of 55 % and a temperature of 22 °C. All experiments were performed using a sphere with diameter $D_0 = 20$ mm, and the depth of the liquid pool was kept fixed at 37 mm [not exactly the same conditions as in Seddon et al. (2012)]. The sphere was released from heights $h_r = 7 - 167$ mm measured from the base of the glass container corresponding to impact speeds $V_0 \approx \sqrt{2gh_r} = 0.4 - 1.8$ m/s. The viscosity of the liquid was varied between 1 mPa s (water) and 1,000 mPa s (Silicon oil, Shin-Etsu Chemical Co. Ltd, Japan), by using water–glycerol mixtures, water–polyvinyl alcohol (PVA) mixtures, and intermediate viscosity silicon oils. The corresponding Stokes numbers are $St = \rho_s D_0 V_0/(9\mu) = O(10 - 10^4)$. Note that since the vapour pressures for these fluids vary from $\sim O(0.1)$ mbar for silicone oils to $\approx$270 mbar for perfluorohexane, we would not expect to see any flow-induced cavitation as $(p_a - p_v)/(\frac{1}{2}\rho_l V_0^2) \geq 1$ for all trials.

3 Experimental observations

In Fig. 2, we present a series of side-view (left column) and bottom-view (right column) images taken during the impact of a 20-mm tungsten carbide sphere with a glass base after being released from rest from the surface of a water pool 37 mm deep. The corresponding velocity of the sphere just before contact (panel 3) in this case was

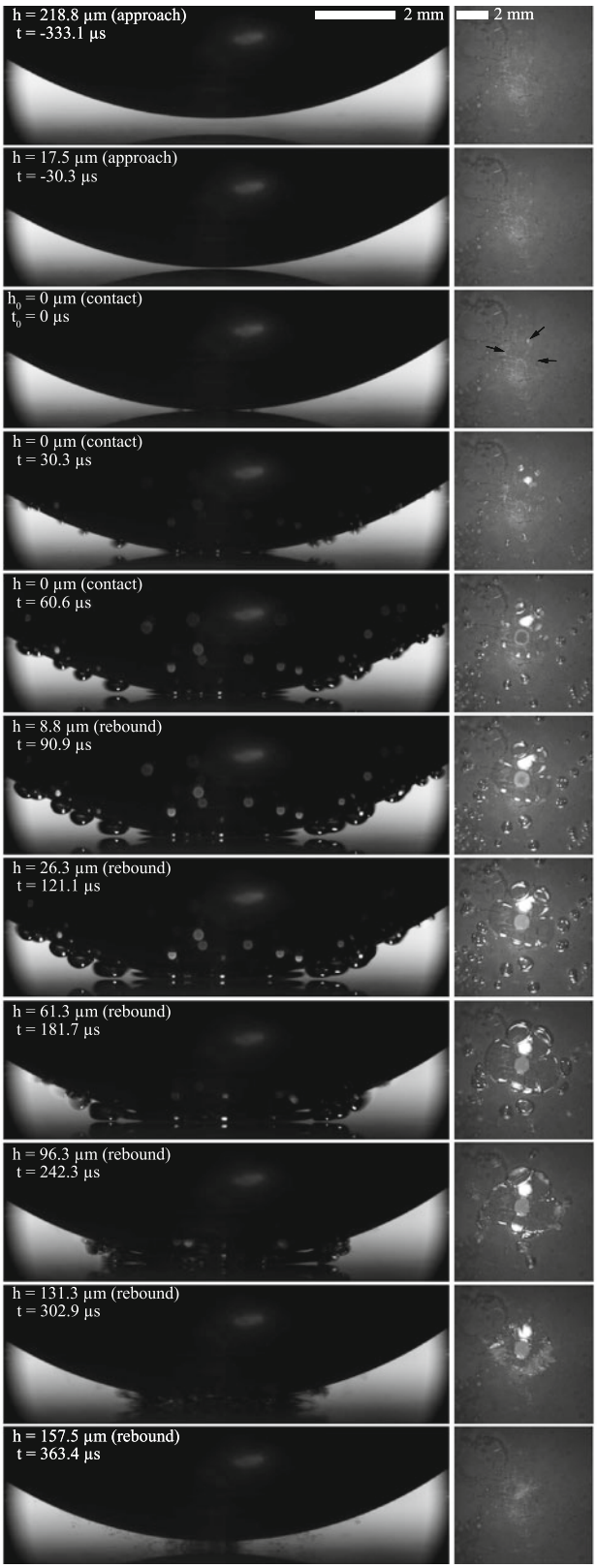

Fig. 2 Impact of a tungsten carbide sphere ($D_0 = 20$ mm) released from (its bottom just touching) the surface of a 37 mm deep pool of water onto a glass plate ($h_r = 37$ mm). The frame at which the sphere makes first contact with the glass base is taken as a reference point ($t_0 = 0$ μs, $h_0 = 0$ μm) and is observed to coincide with the onset of cavitation. h indicates the separation distance between the wall and sphere tip

$u_i = 0.66$ m/s. From the images, we note no sign of cavitation as the sphere approaches the boundary wall. It appears that the experimental results in Seddon et al. (2012) have been misinterpreted, since the parameters used in this realisation fall within those used in Seddon et al. (2012), and thus, we should see cavitation from both views during the approach stage, which is clearly not the case. However, as soon as it touches the wall, small bubbles are observed to originate around the region of contact. We take this as a reference point, $t_0 = 0$ μs and $h_0 = 0$ μm. This contact area has been found in Marston et al. (2011) to be approximately equivalent to the Hertzian contact area, i.e. the area of the nose of the sphere which becomes flattened due to elastic deformation during the true collision period (t = 0–60 μs). During this period, the bubbles rapidly expand in volume and the radial expanse of cavitation increases reaching its maximum ($r_{max} = 6.4$ mm) at 60.6 μs. The sphere then reverses its direction, first observed at $t = 90.9$ μs, upon which the cavitation pattern starts contracting back to the centre. As this happens, the bubbles at the outer extent collapse first and those near to the centre appear to form a distinct cavitation ring. The ring starts moving inwards at $t = 242.3$ μs, and the whole structure disappears completely at 363.4 μs as the sphere moves further away from the wall. In the bottom-view images, a bright white spot observed for $t \geq 30.3$ μs is the reflection of the light source from the bubble surface. The fact that we do not see any such reflections before contact is made is further evidence that cavitation does not occur during the approach or *pressurization* stage.

This qualitative example clearly suggests the liquid to open up in tension due to *depressurization* as the sphere rebounds, in agreement with the conventional theory predicting such phenomenon. In contrast, noticing no sign of bubble formation during sphere approach towards the glass wall (pressurization stage), there is no shear-induced cavitation. Note also that since the sphere is released with its bottom just touching the surface of the pool, we have eliminated the possibility of entrapped bubbles known to be caused by the lubrication pressure in the air (Marston et al. 2011; Thoroddsen et al. 2005). All trials conducted in this manner (i.e. from the surface) resulted in the same

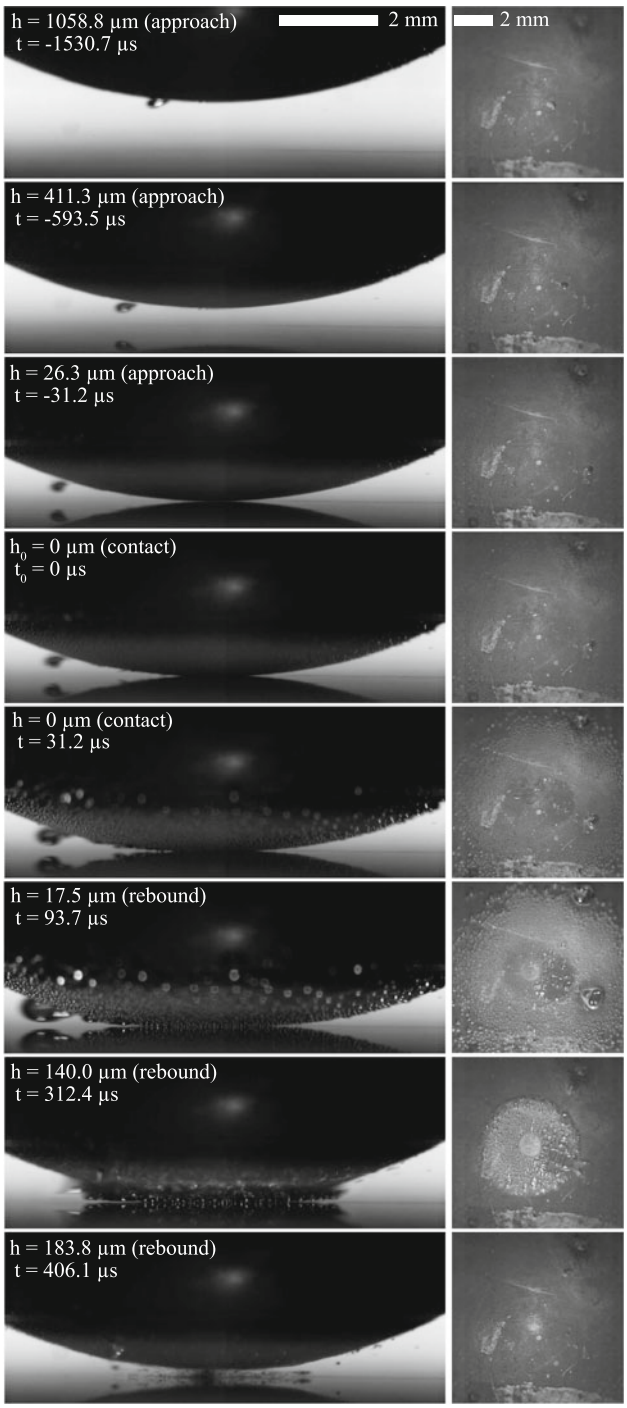

Fig. 3 Impact of a tungsten carbide sphere ($D_0 = 20$ mm) dropped from a height of 42 mm onto a glass plate covered with a 37 mm deep pool of 9 % polyvinyl alcohol (PVA) in water solution (see caption of Fig. 2 for description of the reference point ($t_0 = 0$ µs, $h_0 = 0$ µm) and the variable h). Bubbles can be observed on the sphere surface after initial entry into the liquid layer

observation—namely—that cavitation only occurs *after* the sphere makes contact, never during approach, supporting the observations of Marston et al. (2011) but in clear contradiction to the claim of Seddon et al. (2012), where cavitation was reported to always occur during the approach stage.

In order to assess the possible conditions for shear-induced cavitation during approach, we conducted further experimental trials for higher impact speeds and higher liquid viscosities. Figures 3 and 4 show dual-view image sequences for spheres released from heights of 42 and 57 mm onto a layer of 9 % solution of PVA in water ($\mu = 32.6$ mPa s) and (dimethylpolysiloxane) silicone oil ($\mu = 100$ mPa s), respectively. In both cases, entrained air bubbles are observed at the surface of the sphere after initial entry into the liquid pool. The main bubble entrapped near the bottom tip of the sphere in Fig. 3 is formed by the lubrication pressure of air (Marston et al. 2011; Thoroddsen et al. 2005). Other smaller bubbles can also originate via dynamic wetting (Marston et al. 2011) with viscous liquids as the main (outer) contact line moves up around the sphere. The bubbles in both cases are observed to squeeze radially outwards from the sphere centre acting as flow tracers as the sphere approaches the wall. These bubbles expand due to the drop in pressure after the sphere makes contact. In addition, since the liquid free surface is always exposed to the atmosphere, the possibility of dissolved air in the liquid becoming incorporated into the voids formed during cavitation cannot be neglected, and indeed, we do see evidence of this from the video sequences. However, regardless of whether dissolved gases are present in the liquid film, cavitation still does not occur until the sphere rebounds.

What is clear from these example sequences is that, irrespective of the presence of entrained bubbles and dissolved air in the liquid, we still do not see cavitation during the approach stage, as this would be noticeable by the appearance of other bubbles, which again is not the case. Thus, the liquid does not cavitate during the pressurization stage, whereby the pressure increases as the liquid squeezes in narrowing gap between the sphere and the wall.

In Fig. 5, we plot the separation distance versus time for three different viscosities and mark on the plots the cavitation onset, which always coincides with $h = 0$. In all cases, the sphere was released from a height of 57 mm onto pools of water ($\mu = 1$ mPa s) and silicon oil ($\mu = 100$ and 1,000 mPa s). From these plots, we can determine the velocity just prior to contact (u_i) and just after the direction of motion reverses (u_f). These are shown in Table 1. Again, as indicated by the marks on Fig. 5, cavitation is noticed to onset as soon as $h = 0$ but never before, irrespective of liquid viscosity. Even for the most viscous case, $\mu = 1{,}000$ mPa s, the deceleration of the sphere is insufficient to cause cavitation in itself, until the sphere has essentially reached the point of closest approach. This is again at odds with the report of Seddon et al. (2012),

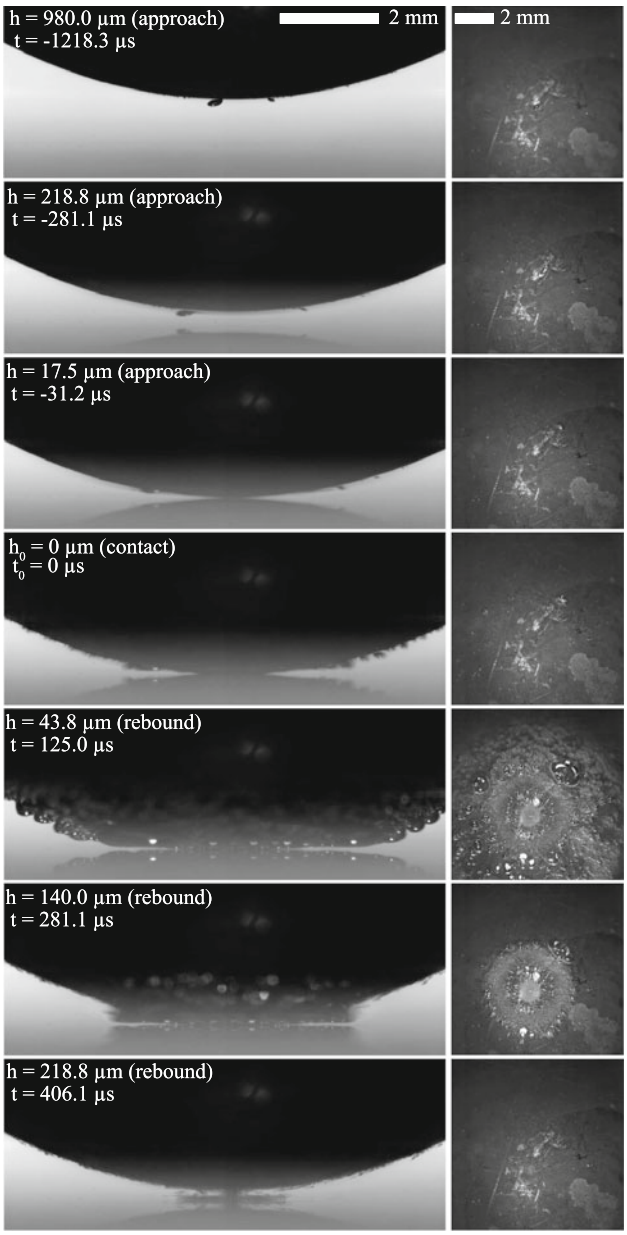

Fig. 4 Impact of a tungsten carbide sphere ($D_0 = 20$ mm) dropped from a height of 57 mm onto a glass plate covered with a 37 mm deep pool of (dimethylpolysiloxane) silicone oil ($\mu = 100$ mPa s). More bubble entrapment is observed as compared to that in Fig. 3 due to a higher liquid viscosity. The liquid cavitates only once at $h = 0$

claiming cavitation to start over 200 µs before contact (or point of closest approach) was reached.

The recent study of Seddon et al. (2012) claiming to show images of shear-induced cavitation bubbles from underneath the sphere excluded the possibility of their origination from a bubble that becomes entrapped by the lubrication pressure of air during sphere entry into the liquid surface by stating that "the trapped bubble would be obliterated during impact and blown outwards to create

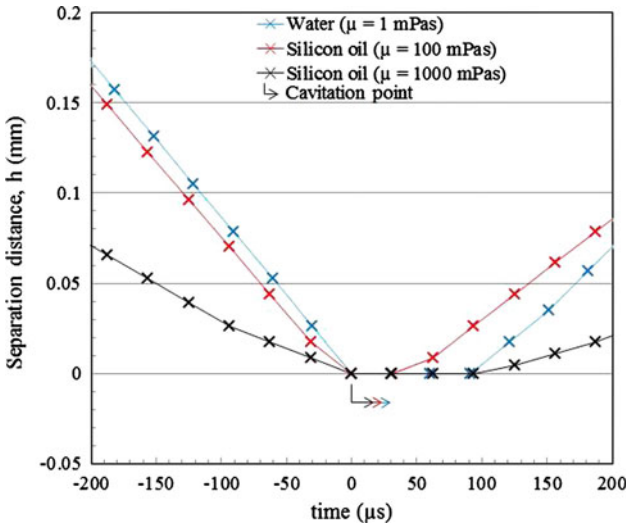

Fig. 5 Separation distance h (mm) versus time t (µs) with marked cavitation points during the impact of a tungsten carbide sphere ($D_0 = 20$ mm) with a glass base covered with a 37 mm deep layer of water (1 mPa s) and silicon oil (100 and 1,000 mPa s). In all runs, the sphere is released from a height of 57 mm above the liquid free surface

Table 1 Close approach (u_i) and rebound speeds (u_f) for realizations in Fig. 5

Liquid	Viscosity (mPa s)	u_i (m/s)	u_f (m/s)
Water	1	0.9	0.69
Silicon oil	100	0.81	0.56
Silicon oil	1,000	0.42	0.17

bubbles centrally at the position of closest approach, *not* as discrete entities on an annulus about this point." Consequences of air entrainment by dynamic wetting of the sphere surface in this regard were not addressed. In Fig. 6, we present the bottom view of a 20-mm-diameter sphere released from a height of 57 mm onto a glass plate covered with a 37 mm layer of silicon oil ($\mu = 1{,}000$ mPa s) at $t = -93.7$ µs before contact ($h = 26.3$ µm). Bubbles entrapped on the sphere surface via lubrication pressure and air entrainment mentioned earlier are found from side views to squeeze radially outwards from the point of closest approach (as in Figs. 3, 4) to produce a distinct annular pattern as the sphere moves towards the wall. These bubbles are never seen for spheres released below the surface, but always seen for the high-viscosity liquids ($\mu = 100$ and 1,000 mPa s) even when released just 5 mm above the liquid surface. In contrast, they are never seen for low-viscosity wetting fluids such as perfluorohexane (C_6F_{14}), whereas for intermediate viscosities (50 % glycerol, $\mu \approx 10$ mPa s, and 9 % PVA, $\mu = 32.6$ mPa s), they are seen for spheres released above the surface, but only

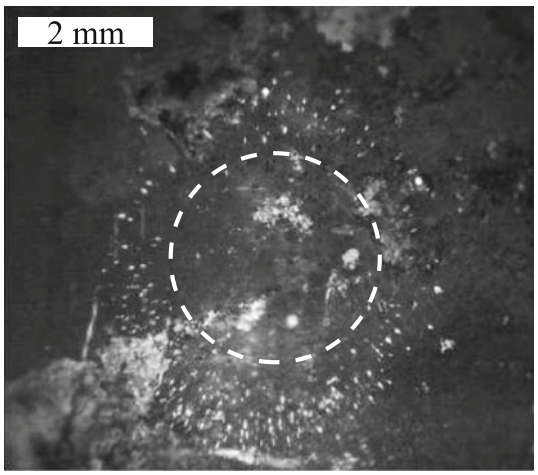

Fig. 6 Annular pattern formed on the sphere surface as bubbles entrapped during the sphere entry into the liquid film squeeze radially out from the point of closest approach. The glass wall is covered with a 37 mm deep layer of silicon oil ($\mu = 1{,}000$ mPa s), and the sphere is dropped from a height of 57 mm. The separation distance between the sphere and wall is $h = 26.3$ μm with $t = -93.7$ μs. The *dashed ring* marks the inner extent of the pattern

above a minimum threshold height. These bubble patterns are remarkably similar to those shown in Seddon et al. (2012).

4 Theoretical considerations

In this section, we present arguments and results from a theoretical model of the motion of a sphere towards a rigid planar surface. The model has previously been described and solved numerically in Uddin et al. (2012), where the approach of the sphere and associated shear-induced viscosity reduction in a Carreau fluid compared favourably to experimental observations. Here, we re-evaluate this model for a Newtonian fluid to assess the shear stress and, in particular, whether this can really overcome the pressure in the fluid given ambient laboratory conditions, as per the experimental conditions.

When the fluid under consideration is modelled as a Newtonian fluid, the governing equations simplify greatly [as opposed to the non-Newtonian case considered in Uddin et al. (2012)]. In this case, the approach of a sphere of radius R_0 towards a solid wall covered by a thin layer of a viscous Newtonian fluid the lubrication approximation can be used to express the radial velocity $u_r(z, r)$ as

$$u_r(r,z) = \frac{-3Vr}{H^3(r)}\left(\left(z - \frac{H(r)}{2}\right)^2 - \left(\frac{H(r)}{2}\right)^2\right) \tag{1}$$

where $H(r) = h + R_0 - (R_0^2 - r^2)^{\frac{1}{2}}$ (with h as the minimum separation of the sphere with the wall) is the height of the

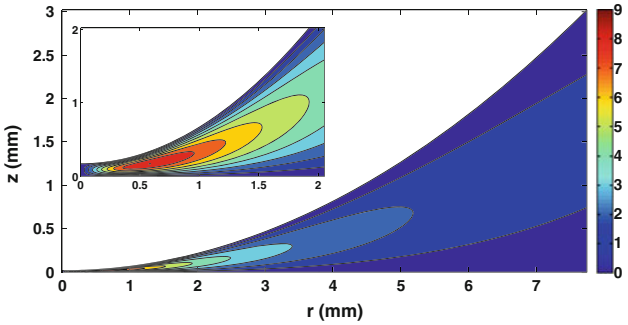

Fig. 7 Numerical computation of the radial velocity u_r as given by (1) corresponding to the flow field when the sphere from Fig. 3 is a distance 17.5 μm from the wall and travelling with velocity 0.7 m/s. The *inset* provides an enlarged view of the close approach region

sphere at a distance r, and V is the velocity of approach (Leal 2007). The squeeze flow between the sphere and the wall induces a tangential shear, S_{11}, which may be written as

$$S_{11} = \mu\frac{\partial u_r}{\partial z} \tag{2}$$

where μ is the viscosity. The pressure is given by

$$P(r) = 6\mu V\int_r^B \frac{\zeta d\zeta}{\left(h + \frac{\zeta^2}{2R_0}\right)^3} + p_a \tag{3}$$

where $p_a = 10^5$ Pa is the ambient pressure, and h is the minimum height of the sphere (or the height at $r = 0$). Here, B is the location at which the pressure in the squeeze flow is set equal to the ambient pressure. In our case, we therefore use the film thickness and the separation height h to determine this value of B [further details about the appropriate choice of this parameter may be found in Uddin et al. (2012)]. We now consider the model for the case of a tungsten carbide sphere of radius 10 mm moving through a film of thickness 37 mm and viscosity 32.6 mPa s as shown in Fig. 3. Using experimental values of the close approach of the sphere to the wall at a distance of 17.5 μm, the sphere velocity is 0.70 m/s. Using these values, we obtain a plot of the radial velocity distribution as shown in Fig. 7.

The criterion for cavitation (Seddon et al. 2012) to occur is that the pressure minus the shear falls below the vapour pressure p_v. This can be written for the 9 % PVA in water solution as

$$P(r) - S_{11} < p_v \approx 2{,}275\,\text{Pa} \tag{4}$$

where the vapour pressure of the solution mixture is obtained using Raoult's Law.

As the sphere approaches the wall, the shear S_{11} will increase dramatically and so will the pressure within the

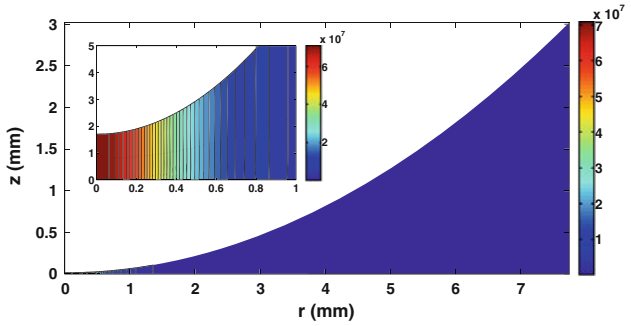

Fig. 8 Numerical computations of the quantity $P(r) - S_{11}$ for values corresponding to Fig. 3 when the sphere is a distance 17.5 μm from the wall and travelling with velocity 0.7 m/s. The minimum value obtained throughout this domain is 8,960 Pa which is above the vapour pressure. An enlarged view of the close approach region is shown in the *inset*

liquid film. As the pressure decays rapidly in the radial direction reaching the ambient pressure near $r = R_0$, it is expected that the shear will eventually overcome the pressure for sufficiently small separation distances. However, in the present case, we see that the distribution of $P(r) - S_{11}$ is given by Fig. 8. The minimum value obtained in this figure is 8,960 Pa which is above the vapour pressure (4), and thus, cavitation is not anticipated in line with the experimental observation in Fig. 3.

5 Concluding remarks

In this communication, we have investigated the onset of cavitation when a sphere impacts a wetted surface. We used a synchronized dual-view high-speed camera system and found the liquid to cavitate at the sphere surface as soon as the direction of motion of the sphere reverses. This observation is in agreement with the conventional theory which associates cavitation with the depressurization stage as the sphere rapidly decelerates upon contact and then rebounds. Bubble entrapment was noticed on the sphere surface when released from above the liquid surface. This is known to be caused by two different mechanisms; the lubrication pressure of air and dynamic wetting (for viscous liquids) as the contact line moves up around the sphere. Hence, for trials with viscous liquids, multiple bubbles were entrapped during entry which were squeezed radially outwards from the sphere centre as it approached the wall. This was found to produce an annular structure which appears to be very similar to the observations of Seddon et al. (2012). Noting that our parameter space herein and those of Marston et al. (2011a, b), Uddin et al. (2012) fall within that of Seddon et al. (2012), we *should* have observed cavitation during the approach stage in *all* of our current and previous experiments based on the claim of Seddon et al. (2012), but this is clearly not the case. We note, however, for experiments performed at reduced ambient pressures, close to the vapour pressure of the liquid ($p_v \approx 25$ mbar for water), one would expect to see cavitation during approach if $(p_a - p_v)/(\frac{1}{2}\rho_l V_0^2) \leq 1$. Thus, for ambient pressures, say $p_a = 30$ mbar, one would only need an impact speed of approximately $V_0 \approx 1$ m/s to see flow-induced cavitaton in water.

References

Barnocky G, Davis RH (1988) Elastohydrodynamic collision and rebound of spheres: experimental verification. Phys Fluids 31:1324–1329

Brenner H (1961) The slow motion of a sphere through a viscous fluid towards a plane surface. Chem Eng Sci 16:242–251

Chen YL, Israelachvili J (1991) New mechanism of cavitation damage. Science 252:1157–1160

Davis RH, Serayssol JM, Hinch EJ (1986) The elastohydrodynamic collision of two spheres. J Fluid Mech 163:479–497

Davis RH, Rager DA, Good BT (2002) Elastohydrodynamic rebound of spheres from coated surfaces. J Fluid Mech 468:107–119

Joseph DD (1998) Cavitation and the state of stress in a flowing liquid. J. Fluid Mech 366:367–378

Kuhl T, Ruths M, Chen Y, Israelachvili J (1994) Direct visualization of cavitation and damage in ultrathin liquid films. J. Heart Valve Dis 3(Suppl. I):117–127

Leal LG (2007) Advanced transport phenomena: fluid mechanics and convective transport processes. Cambridge University Press, Cambridge

Marston JO, Yong W, Thoroddsen ST (2010) Direct verification of the lubrication force on a sphere travelling through a viscous film upon approach to a solid wall. J Fluid Mech 655:515–526

Marston JO, Yong W, Ng WK, Tan RBH, Thoroddsen ST (2011a) Cavitation structures formed during the rebound of a sphere from a wetted surface. Exp Fluids 50:729–746

Marston JO, Vakarelski IU, Thoroddsen ST (2011b) Bubble entrapment during sphere impact onto quiescent liquid surfaces. J Fluid Mech 680:660–670

Seddon JRT, Kok MP, Linnartz EC, Lohse D (2012) Bubble puzzles in liquid squeeze: cavitation during compression. Europhys Lett 97:24004

Thoroddsen ST, Etoh TG, Takehara K, Ootsuka N, Hatsuki Y (2005) The air bubble entrapped under a drop impacting on a solid surface. J Fluid Mech 545:203–212

Uddin J, Marston JO, Thoroddsen ST (2012) Squeeze flow of a Carreau fluid during sphere impact. Phys Fluids 24:073104